MIT Libraries | DSpace@MIT

MIT Open Access Articles

Structure of a Magnetic Flux Annihilation Layer Formed by the Collision of Supersonic, Magnetized Plasma Flows

Massachusetts Institute of Technology

Structure of a Magnetic Flux Annihilation Layer Formed by the Collision of Supersonic, Magnetized Plasma Flows

L. G. Suttle,[1,*] J. D. Hare,[1] S. V. Lebedev,[1,†] G. F. Swadling,[1,‡] G. C. Burdiak,[1] A. Ciardi,[2,3] J. P. Chittenden,[1]
N. F. Loureiro,[4] N. Niasse,[1] F. Suzuki-Vidal,[1] J. Wu,[5] Q. Yang,[6] T. Clayson,[1] A. Frank,[7] T. S. Robinson,[1]
R. A. Smith,[1] and N. Stuart[1]

[1]*Blackett Laboratory, Imperial College, London SW7 2BW, United Kingdom*
[2]*Sorbonne Universités, UPMC Universités Paris 6, UMR 8112, LERMA, Paris F-75005, France*
[3]*LERMA, Observatoire de Paris, PSL Research University, CNRS, UMR 8112, Paris F-75014, France*
[4]*Plasma Science and Fusion Center, Massachusetts Institute of Technology, Cambridge, Massachusetts 02139, USA*
[5]*State Key Laboratory of Electrical Insulation and Power Equipment, Xi'an Jiaotong University, Xi'an 710049, China*
[6]*Institute of Fluid Physics, China Academy of Engineering Physics, Mianyang 621900, China*
[7]*Department of Physics and Astronomy, University of Rochester, Rochester, New York 14627, USA*
(Received 22 January 2016; published 31 May 2016)

We present experiments characterizing the detailed structure of a current layer, generated by the collision of two counterstreaming, supersonic and magnetized aluminum plasma flows. The antiparallel magnetic fields advected by the flows are found to be mutually annihilated inside the layer, giving rise to a bifurcated current structure—two narrow current sheets running along the outside surfaces of the layer. Measurements with Thomson scattering show a fast outflow of plasma along the layer and a high ion temperature ($T_i \sim \bar{Z}T_e$, with average ionization $\bar{Z} = 7$). Analysis of the spatially resolved plasma parameters indicates that the advection and subsequent annihilation of the inflowing magnetic flux determines the structure of the layer, while the ion heating could be due to the development of kinetic, current-driven instabilities.

The interaction of supersonic, counterstreaming plasma flows occurs in many astrophysical scenarios (e.g., astrophysical jets [1] and termination shocks [2,3]) and in laboratory experiments (e.g., colliding plasmas in inertial confinement fusion hohlraums [4]). The presence of frozen-in magnetic fields advected by the colliding flows could play an important role in determining the structure of the interaction region in these systems. Collisions of magnetized plasmas with oppositely directed magnetic fields should eventually lead to annihilation of the flux via magnetic reconnection. In many astrophysical scenarios reconnection occurs in high beta plasmas and is strongly driven, with ram pressure significantly exceeding the magnetic pressure. The structure of the reconnection layer in these conditions is unknown, but is expected to adjust to accommodate the rate of magnetic flux delivered into the layer, where, for example, a pileup of the magnetic flux could contribute to controlling the reconnection rate [5,6]. A number of recent laser-driven, high energy density physics (HEDP) experiments [7–10] have investigated magnetic reconnection in the strongly driven regime, as well as the formation of astrophysically relevant collisionless shocks [11] and self-organized field structures [12]. Large-scale field structures produced by collisions between laser-driven plasma flows have, for example, been interpreted [11] as being due to the accumulation of advected toroidal magnetic fields generated via the Biermann battery mechanism at the laser spots [13]. Despite the importance of magnetic fields in

defining the properties of shocks formed in HEDP plasmas, experimental information is still limited.

In this Letter we present experimental data characterizing the structure of an interaction layer formed by the collision of two counterstreaming, supersonic (sonic Mach number $M_S > 3$), magnetized plasma flows. These flows advect embedded magnetic fields (magnetic Reynolds number $\mathrm{Re}_M > 30$), orientated in opposing directions perpendicular to the flow, and their interaction is strongly driven [i.e., high dynamic beta regime, $\beta_{\mathrm{dyn}} = \rho V_{\mathrm{flow}}^2/(B^2/2\mu_0) \sim 7$]. The experiments provide detailed, simultaneous, spatially resolved measurements of the key plasma parameters: flow velocities and temperatures via Thomson scattering (TS), the distribution of the magnetic field via polarimetry, and the electron density distribution via laser interferometry. We observe the formation of a thin current layer (half thickness $\delta \approx 0.5$ mm, comparable to the ion inertial length c/ω_{pi}), which is supported by the balance between the ram pressure of the flow and the thermal pressure inside the layer, for a time significantly exceeding the expected characteristic hydrodynamic time scale ($\tau_{\mathrm{layer}} > 20\delta/V_{\mathrm{flow}}$). The measured magnetic field distribution indicates that the destruction of magnetic flux takes place at the layer surfaces, consistent with two narrow, localized current sheets. Measurements also show a high ion temperature in the layer ($T_i \sim \bar{Z}T_e$, with $\bar{Z} \sim 7$).

The experiments were carried out at the MAGPIE pulsed power facility [14] using the setup illustrated in Figs. 1(a)
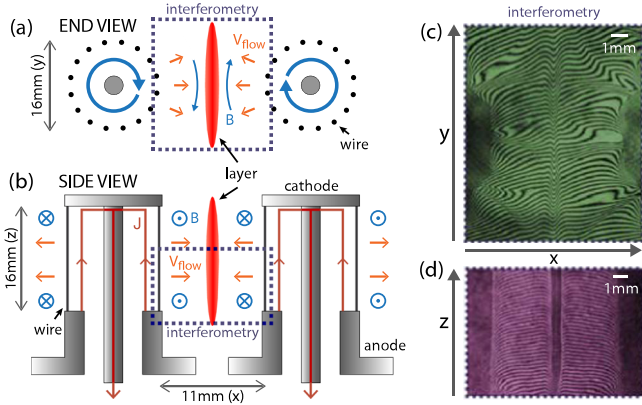
FIG. 1.   Cross-sectional schematic diagrams of the production of two magnetized, colliding plasma flows from (a) end and (b) side views. [(c) and (d)] Corresponding interferograms of the structure of the interaction region from each perspective (fields of view are indicated in schematics).

and 1(b). The supersonic counterstreaming plasma flows are produced by the ablation of thin aluminum (Al) wires driven by a 1.4 MA, 250 ns rise-time current pulse. These are arranged to form two cylindrical "exploding" wire arrays [15], with the total current equally divided between the two arrays. The current J in each array runs up the wires and returns through the central conductor, as indicated in Fig. 1(a). Ablation flows form in a similar manner to those produced by standard ("imploding") wire arrays [16–18]; however, here the $J \times B$ force acts to direct the plasma radially outwards, into a region initially free of magnetic fields. The ablated plasma is accelerated away from the wires, reaching a velocity of ∼50 km/s within the first 1–2 mm, and thereafter propagates with an almost constant velocity. Previous measurements [19,20] have demonstrated that the plasma flows generated by a single exploding wire array have a frozen-in, azimuthal, advected magnetic field ($B \sim 2T$), and are super-fast-magnetosonic. The arrays used in the current experiments consist of 16, 40 μm-diameter Al wires, 16 mm in length, positioned on a 16 mm diameter [Fig. 1(a)]. The gap between the two arrays is 11 mm and they are driven in the same polarity, such that when the advected magnetic fields meet they are oriented in opposite directions, and their interaction should lead to the annihilation of the magnetic flux.

The interaction of the colliding plasmas was diagnosed using a range of diagnostics, allowing simultaneous measurements of the relevant plasma parameters with high spatial and temporal resolution. A TS diagnostic [20,21] was used to record the ion feature of the collective TS spectrum, measuring the flow velocity and temperatures (T_i, $\bar{Z}T_e$) of the plasma. The distribution of the magnetic field was measured using a polarimetry (Faraday rotation) diagnostic (1053 nm and 1 ns) [20], while the electron density was obtained in end-on (x-y) and side-on (x-z) directions via laser interferometry (532 and 355 nm, 0.3 ns, 1053 nm, and 1 ns) [20,22].

Typical end-on and side-on interferograms obtained at $t = 215$ ns after the current start, when the interaction layer is fully formed, are shown in Figs. 1(c) and 1(d). In this Letter we concentrate on the detailed characterization of the layer properties at this time. Measurements were performed at various times between $t = 160$ ns, when the layer becomes detectable by interferometry (electron line density $\int n_e dl$ corresponding to a ½-fringe shift), and $t = 265$ ns, when the drive current has passed its peak. These measurements indicated that while the density of the accumulated plasma increases with time, the overall structure of the layer and its thickness ($2\delta \sim 1$ mm) remain constant. The interferograms are processed into maps of $\int n_e dl$ by applying the analysis procedure described in [20,22]. For the end-on data the maps can be further converted to electron density n_e, by dividing $\int n_e dl$ by the probing path length (i.e., array height), on the basis that the density structure is approximately uniform in the axial (z) direction.

The end-on electron density map [Fig. 2(a) and the raw image in Fig. 1(c)] shows the radially diverging plasma flows produced by the wire arrays for the region indicated in Fig. 1(a). The ablated plasma density close to each array is modulated azimuthally due to the use of a relatively small number of wires in these experiments (16 per array). The observed flow structure, however, evolves downstream of the wires via the oblique collision of the individual streams (as described in [19,22]), smoothing out these modulations in the region just upstream of the interaction layer. Comparison of radial profiles of the density at analogous azimuthal positions (e.g., profiles marked "1" and "2") shows that the upstream flow structure is not affected by the subsequent interaction, as should be expected for a supersonic flow. The collision of the opposing flows leads to the formation of a dense, axially smooth, narrow layer in the midplane, extending across the length of the image in the y direction, perpendicular to the flow. Within the layer, it is noted that the maximum density is not located at the central position ($x,y = 0$), despite the fact it receives the highest influx of material from the flows. This is due to a
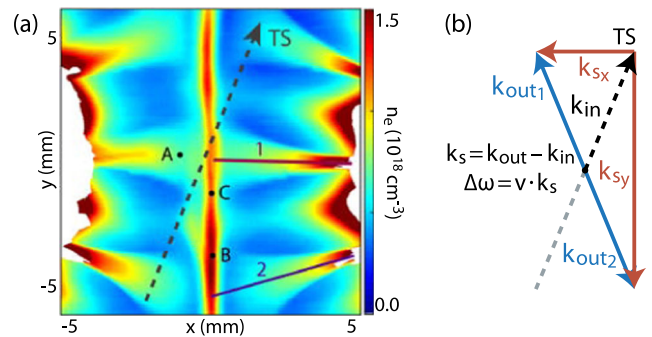

FIG. 2.   (a) End-on electron density map, obtained by interferometry, showing probing geometry of the TS laser beam, and positions (black dots, A-C) of TS measurements whose spectra are shown in Fig. 3. (b) TS geometry vector diagram.

symmetric outward plasma motion along the layer, which we directly measure using Thomson scattering.

The multipoint TS diagnostic, whose geometry is illustrated in Fig. 2, operated simultaneously with the interferometry measurements. The focused probing laser beam (532 nm, 5 ns FWHM, 3J, $\emptyset < 200\ \mu$m) propagated in the x-y plane, at an angle of 22.5° to the interaction layer. The position (y coordinate) at which the probing beam crossed the layer was adjusted between different experiments to sample different regions of the plasma. The scattered light was collected in the same plane, from 13 spatial positions along the beam, at scattering angles of $\theta = 45$° and 135° to the laser, using an imaging spectrometer and two linear arrays of optical fibers (see [20,21] for more details). Alignment of the TS diagnostic and determination of the scattering volume locations with respect to the interferogram was performed as described in [20], with a precision of ≤0.2 mm. The scattering geometry [Fig. 2(b)] produces separate measurements sensitive to the components of the flow velocity perpendicular (V_x) and parallel (V_y) to the interaction layer, respectively. These are determined from the Doppler shift of the TS spectra as $\delta\omega_{D1} = k_{Sx}V_x$ and $\delta\omega_{D2} = k_{Sy}V_y$.

Characteristic TS spectra from three key spatial positions in the interaction are shown in Figs. 3(a)–3(c). These spectra were recorded simultaneously with the interferometry data presented in Fig. 2(a) and their positions are marked in that figure (A-C, with black dots representing the spatial resolution of the measurements). The TS data obtained upstream of the layer [e.g., position A, spectrum Fig. 3(a)] indicate that the flows approach the interaction layer with an incident velocity of approximately 50 km/s in the direction normal to the layer. On crossing the layer
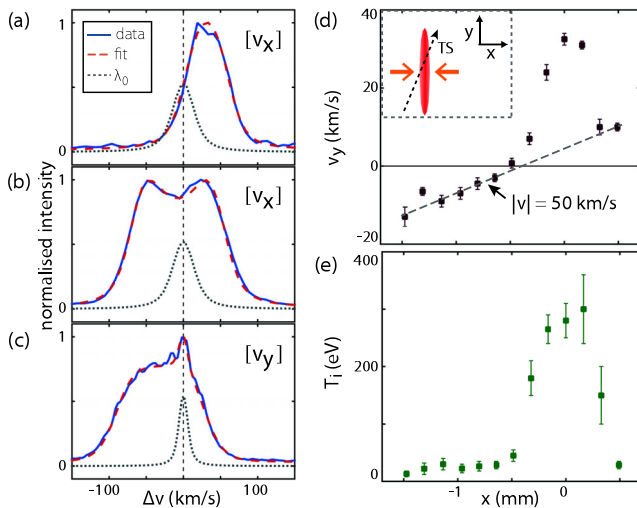
boundary, this V_x component falls to 0 [e.g., as shown in Fig. 3(b)]; however, we see that the plasma inside the interaction layer acquires significant motion in the perpendicular y direction [e.g., Fig. 3(c)]. Measurements at positions C ($y = -1.0$ mm) and B ($y = -3.7$ mm) yield $V_y = -30$ km/s and -60 km/s, respectively, indicating an outward acceleration of material along the layer. Figure 3(d) illustrates this motion in comparison to the plasma outside of the layer; V_y is plotted as a function of x for the 13 scattering positions along the probing TS beam in a single experiment [with the beam passing through position C in Fig. 2(a)]. This shows that there is a clear perturbation within the layer from the linear velocity profile (dashed line) of the upstream plasma—this nonzero upstream V_y profile being due to the cylindrical divergence of the setup [Fig. 1(a)].

Fitting theoretical form factors to the measured TS spectra (similar to [20,23]) allows us to obtain plasma temperatures [Fig. 3(e)]. We note that local temperatures obtained from fits to the spectra from each of the separate scattering directions [Fig. 2(b)] were in agreement. This strongly suggests that the shape of the scattering spectra is determined by thermal motion, and not by possible variations of the flow velocities inside the scattering volumes. The upstream plasma was found to be cold ($T_i = 22 \pm 10$ eV, $T_e < 20$ eV), while inside the layer the ion temperature rises rapidly, reaching $T_i \approx 300$ eV at the most centrally measured position (C). The electron temperature in the layer is best determined from the spectra obtained for the 45° scattering angle [e.g., Fig. 3(b)], yielding $\bar{Z}T_e = 320 \pm 20$ eV. Using this measured value to constrain the magnitude of the product, a nonlocal thermodynamic equilibrium model [24,25] can then be applied to calculate self-consistent values of $\bar{Z}$ and T_e, which provides a best estimate of average ionization $\bar{Z} = 7.3$ and $T_e = 43$ eV. We emphasize that in all experiments the measured ion temperature significantly exceeded the electron temperature inside the layer, with $T_i \sim \bar{Z}T_e$.

The distribution of the magnetic field was measured using simultaneous side-on polarimetry and interferometry. Polarimetry images were taken using two channels with oppositely rotated linear polarizers at ± 3° from extinction. The Faraday rotation images were analyzed using the procedure described in detail in [20], yielding a two-dimensional map of the rotation angle $\alpha(x, z)$ as shown in Fig. 4(b). It is seen that the rotation angle has different signs on the two sides of the layer, as expected for the magnetic field geometry of this setup [Fig. 1(b)]. The Faraday rotation angle is determined by both the magnetic field and electron density [26]. The average magnetic field in the y direction can be found by dividing the rotation angle by the line density,

FIG. 3.   [(a)–(c)] Fitted TS spectra for the three spatial points in the interaction region marked in Fig. 2(a). The dotted line (λ_0) indicates spectrometer resolution. [(d) and (e)] Profiles of $V_y(x)$ and $T_i(x)$ measured in a single experiment for scattering volumes along the TS beam when passing through position C in Fig. 2(a).

$$B_y(x, z) = \frac{8\pi^2 \varepsilon_0 m_e^2 c^3}{e^3 \lambda^2} \frac{\alpha(x, z)}{\int [n_e(x, y, z)dy]}, \quad (1)$$
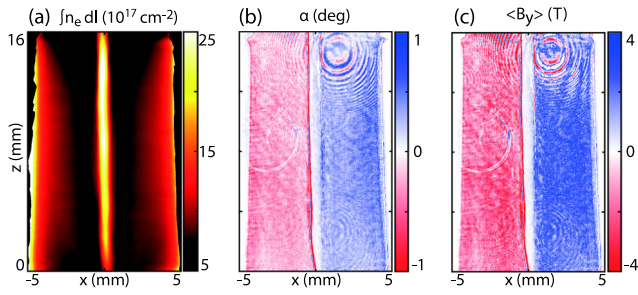
FIG. 4.   Side-on maps of the interaction region showing (a) the electron line density (interferometry), (b) Faraday rotation angle, and (c) magnetic field. Ring structures evident in the data are artifacts caused by dust spots.

and the resulting map is shown in Fig. 4(c). The distribution of the magnetic field is approximately uniform in the z direction, with some noise on smaller spatial scales due to the small values of the Faraday rotation angle ($\sim 1°$). To reduce the effect of the noise we average in the z direction over an interval of $\Delta z = 6$ mm in the middle of the image to produce the magnetic field profile of Fig. 5(a). Outside the interaction layer $B = \pm 2T$; the field then peaks in a narrow interval at the layer's surface before rapidly dropping to almost 0 inside. The corresponding current density distribution ($j_z = -1/\mu_0 \, \partial B_y/\partial x$) consists of two, narrow, bidirectional current sheets located at the boundaries of the layer [Fig. 5(b)]. This field structure is consistent with the compression of the advected magnetic field at the shock, followed by a rapid dissipation of the magnetic flux in a narrow (≈ 0.1 mm) region at the boundary of the layer. The mean free paths for electrons and ions in the plasma are much shorter than the spatial scales involved ($\lambda_{ii} \sim \lambda_{ei} \sim 3 \mu$m), suggesting the plasma is strongly collisional. The magnetic field pileup occurs at $|x| \sim 0.5$ mm, which is comparable to the ion skin depth $c/\omega_{pi} \sim 0.3$–0.4 mm. This suggests that two-fluid physics such as the Hall effect plays an important role in this system, as the ions decouple from the electrons on the scale at which we see flux pileup.

The plasma layer formed in these experiments appears to be in dynamic equilibrium, maintaining an approximately constant thickness over a time scale much longer than the
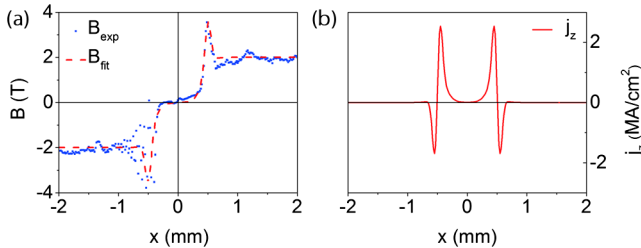

FIG. 5.   (a) z-averaged profile of the measured (blue dots) magnetic field $B_y(x)$, and (b) profile of the current density calculated for a fitted magnetic field profile shown by the red dashed line in (a).

characteristic hydrodynamic time. Using the measured plasma parameters we find that there is a close balance between the ram pressure of the incoming flow and the thermal pressure of the plasma in the layer, and also between the ram pressure and the magnetic pressure of the piled-up field. We note that the magnetic pressure is not important in the upstream flow [$\rho V^2/(B^2/2\mu_0) = 2M_A^2 \sim 7$], nor inside the layer, where the magnetic pressure is negligible in comparison to thermal pressure.

The energy balance presents a more complicated and interesting situation due to an unexpectedly high ion temperature ($T_i \approx 300$ eV) inside the layer. The 50 km/s velocity measured upstream of the layer boundary, where T_i is small, corresponds to Al ions with a directed kinetic energy of $E_i = 340$ eV. Thermalization of this kinetic energy (assuming no energy is transferred to the electrons) gives a maximum possible ion temperature of $T_i = (2/3)E_i = 230$ eV. This is already smaller than the measured postinteraction T_i. The time for energy exchange between the electron and ion populations, $\tau_{ei}^{E} \sim 20$ ns, is much shorter than the lifetime of the layer and should lead to $T_i \sim T_e$ and not $T_i \sim \bar{Z}T_e$. The expected postshock plasma temperature corresponding to equilibration between the ion and electron temperatures can be estimated using a standard expression for heating in a strong shock [27],

$$k_B T = E_i \frac{4(\gamma - 1)}{(\gamma + 1)^2} \frac{1}{(\bar{Z} + 1)}. \tag{2}$$

Using $\gamma = 5/3$ yields a much lower temperature of $T_i = T_e \sim 30 \rightarrow 15$ eV for $\bar{Z} = 3 \rightarrow 7$, while the immediate postshock ion temperature is $T_i \sim 120$ eV, corresponding to $\bar{Z} = 0$ in the above formula.

These estimates suggest that the postshock ion temperature should be significantly smaller than measured, even without taking into account energy losses to ionization and radiative cooling. This in turn suggests that there must be a mechanism providing continuous heating of the ions, in order to sustain both their high temperature and the large difference between the ion and electron temperatures.

The most plausible explanation for the observed ion heating is that it occurs in the current sheets formed at the boundaries of the layer. The large spatial gradients of the magnetic field seen in this region (Fig. 5) correspond to current densities of the order of ~ 1–2 MA/cm^2; however, resistive heating of the plasma by this current should only heat the electrons, and the subsequent transfer of energy to the ions cannot explain the observed $T_i \sim \bar{Z}T_e \gg T_e$. Enhanced heating of the ions has been extensively discussed, e.g., in the context of magnetic reconnection studies [28–31], and is often associated with the development of current-driven kinetic plasma turbulence. The high current density at the boundary of the current layer corresponds to a velocity of the current-carrying electrons ($u_{ez} = j_z/en_e$) exceeding the ion sound speed ($u_{ez}/C_S \sim 5$). This could lead

to the development of, e.g., ion-acoustic or lower hybrid drift instabilities [32], but additional experiments are needed to investigate this further.

In summary, these experiments have provided a detailed characterization of the interaction layer formed by the collision of two counterstreaming, magnetized, supersonic plasma flows with oppositely oriented magnetic fields. We find that the pileup, and the subsequent dissipation of magnetic flux, occurs in a narrow region at the boundaries of the interaction layer, forming a bifurcated current structure. The layer has a half thickness of $\delta \sim c/\omega_{\mathrm{pi}}$, and is supported in a quasisteady state by the balance between the ram pressure of the incoming flow and the thermal pressure in the layer. Thomson scattering measurements of the plasma parameters show that the plasma inside the layer moves outwards, along the B field of the incoming plasma flows, with a speed comparable to the inflow velocity. The measured ion temperature is unexpectedly high in comparison with the electron temperature, a situation incompatible with purely resistive heating. It is possible that the observed strong ion heating is driven by the development of kinetic instabilities in the current sheet, but the exact mechanism responsible for this is unknown at present.

[*]l.suttle10@imperial.ac.uk

[†]s.lebedev@imperial.ac.uk

[‡]Present address: Lawrence Livermore National Laboratory, California 94550, USA.

 [1] P. Hartigan, A. Frank, J. M. Foster, B. H. Wilde, M. Douglas, P. A. Rosen, R. F. Coker, B. E. Blue, and J. F. Hansen, Fluid dynamics of stellar jets in real time: Third epoch hubble space telescope images of HH 1, HH 34, and HH 47, Astrophys. J. **736**, 29 (2011).

 [2] M. Opher, J. F. Drake, M. Swisdak, K. M. Schoeffler, J. D. Richardson, R. B. Decker, and G. Toth, Is the magnetic field in the heliosheath laminar or a turbulent sea of bubbles?, Astrophys. J. **734**, 71 (2011).

 [3] J. Pétri and Y. Lyubarsky, Magnetic reconnection at the termination shock in a striped pulsar wind, Astron. Astrophys. **473**, 683 (2007).

 [4] J. Lindl, Development of the indirect-drive approach to inertial confinement fusion and the target physics basis for ignition and gain, Phys. Plasmas **2**, 3933 (1995).

 [5] D. Biskamp, Magnetic reconnection via current sheets, Phys. Fluids **29**, 1520 (1986).

 [6] W. Fox, A. Bhattacharjee, and K. Germaschewski, Fast Magnetic Reconnection in Laser-Produced Plasma Bubbles, Phys. Rev. Lett. **106**, 215003 (2011).

 [7] G. Fiksel, W. Fox, A. Bhattacharjee, D. H. Barnak, P.-Y. Chang, K. Germaschewski, S. X. Hu, and P. M. Nilson, Magnetic Reconnection between Colliding Magnetized Laser-Produced Plasma Plumes, Phys. Rev. Lett. **113**, 105003 (2014).

 [8] M. J. Rosenberg, C. K. Li, W. Fox, I. Igumenshchev, F. H. Séguin, R. P. J. Town, J. A. Frenje, C. Stoeckl, V. Glebov, and R. D. Petrasso, A laboratory study of asymmetric magnetic reconnection in strongly driven plasmas, Nat. Commun. **6**, 6190 (2015).

 [9] M. J. Rosenberg, C. K. Li, W. Fox, A. B. Zylstra, C. Stoeckl, F. H. Séguin, J. A. Frenje, and R. D. Petrasso, Slowing of Magnetic Reconnection Concurrent with Weakening Plasma Inflows and Increasing Collisionality in Strongly Driven Laser-Plasma Experiments, Phys. Rev. Lett. **114**, 205004 (2015).

[10] P. M. Nilson, L. Willingale, M. C. Kaluza, C. Kamperidis, S. Minardi, M. S. Wei, P. Fernandes, M. Notley, S. Bandyopadhyay, M. Sherlock, R. J. Kingham, M. Tatarakis, Z. Najmudin, W. Rozmus, R. G. Evans, M. G. Haines, A. E. Dangor, and K. Krushelnick, Magnetic Reconnection and Plasma Dynamics in Two-Beam Laser-Solid Interactions, Phys. Rev. Lett. **97**, 255001 (2006).

[11] H.-S. Park, C. M. Huntington, F. Fiuza, R. P. Drake, D. H. Froula, G. Gregori, M. Koenig, N. L. Kugland, C. C. Kuranz, D. Q. Lamb, M. C. Levy, C. K. Li, J. Meinecke, T. Morita, R. D. Petrasso, B. B. Pollock, B. A. Remington, H. G. Rinderknecht, M. Rosenberg, J. S. Ross, D. D. Ryutov, Y. Sakawa, A. Spitkovsky, H. Takabe, D. P. Turnbull, P. Tzeferacos, S. V. Weber, and A. B. Zylstra, Collisionless shock experiments with lasers and observation of Weibel instabilities, Phys. Plasmas **22**, 056311 (2015).

[12] N. L. Kugland, D. D. Ryutov, P.-Y. Chang, R. P. Drake, G. Fiksel, D. H. Froula, S. H. Glenzer, G. Gregori, M. Grosskopf, M. Koenig, Y. Kuramitsu, C. Kuranz, M. C. Levy, E. Liang, J. Meinecke, F. Miniati, T. Morita, A. Pelka, C. Plechaty, R. Presura, A. Ravasio, B. A. Remington, B. Reville, J. S. Ross, Y. Sakawa, A. Spitkovsky, H. Takabe, and H.-S. Park, Self-organized electromagnetic field structures in laser-produced counterstreaming plasmas, Nat. Phys. **8**, 809 (2012).

[13] K. M. Schoeffler, N. F. Loureiro, R. A. Fonseca, and L. O. Silva, Magnetic-Field Generation and Amplification in an Expanding Plasma, Phys. Rev. Lett. **112**, 175001 (2014).

[14] I. H. Mitchell, J. M. Bayley, J. P. Chittenden, J. F. Worley, A. E. Dangor, M. G. Haines, and P. Choi, A high impedance mega-ampere generator for fiber z-pinch experiments, Rev. Sci. Instrum. **67**, 1533 (1996).

[15] A. J. Harvey-Thompson, S. V. Lebedev, S. N. Bland, J. P. Chittenden, G. N. Hall, A. Marocchino, F. Suzuki-Vidal, S. C. Bott, J. B. A. Palmer, and C. Ning, Quantitative analysis of plasma ablation using inverse wire array Z pinches, Phys. Plasmas **16**, 022701 (2009).

[16] S. V. Lebedev, F. N. Beg, S. N. Bland, J. P. Chittenden, A. E. Dangor, M. G. Haines, K. H. Kwek, S. A. Pikuz, and T. A. Shelkovenko, Effect of discrete wires on the implosion dynamics of wire array Z pinches, Phys. Plasmas **8**, 3734 (2001).

[17] J. Greenly, M. Martin, I. Blesener, D. Chalenski, P. Knapp, R. McBride, B. R. Kusse, and D. a. Hammer, The role of flux advection in the development of the ablation streams

and precursors of wire array Z-pinches, AIP Conf. Proc. **1088**, 53 (2009).

[18] V. V. Aleksandrov, V. A. Barsuk, E. V. Grabovski, A. N. Gritsuk, G. G. Zukakishvili, S. F. Medovshchikov, K. N. Mitrofanov, G. M. Oleinik, and P. V. Sasorov, Studies of penetration of the magnetic field into electrically imploded loads in the Angara-5-1 facility, Plasma Phys. **35**, 200 (2009).

[19] S. V. Lebedev, L. Suttle, G. F. Swadling, M. Bennett, S. N. Bland, G. C. Burdiak, D. Burgess, J. P. Chittenden, A. Ciardi, A. Clemens, P. de Grouchy, G. N. Hall, J. D. Hare, N. Kalmoni, N. Niasse, S. Patankar, L. Sheng, R. A. Smith, F. Suzuki-Vidal, J. Yuan, A. Frank, E. G. Blackman, and R. P. Drake, The formation of reverse shocks in magnetized high energy density supersonic plasma flows, Phys. Plasmas **21**, 056305 (2014).

[20] G. F. Swadling, S. V. Lebedev, G. N. Hall, S. Patankar, N. H. Stewart, R. A. Smith, A. J. Harvey-Thompson, G. C. Burdiak, P. de Grouchy, J. Skidmore, L. Suttle, F. Suzuki-Vidal, S. N. Bland, K. H. Kwek, L. Pickworth, M. Bennett, J. D. Hare, W. Rozmus, and J. Yuan, Diagnosing collisions of magnetized, high energy density plasma flows using a combination of collective Thomson scattering, Faraday rotation, and interferometry (invited), Rev. Sci. Instrum. **85**, 11E502 (2014).

[21] G. F. Swadling, S. V. Lebedev, A. J. Harvey-Thompson, W. Rozmus, G. C. Burdiak, L. Suttle, S. Patankar, R. A. Smith, M. Bennett, G. N. Hall, F. Suzuki-Vidal, and J. Yuan, Interpenetration, Deflection, and Stagnation of Cylindrically Convergent Magnetized Supersonic Tungsten Plasma Flows, Phys. Rev. Lett. **113**, 035003 (2014).

[22] G. F. Swadling, S. V. Lebedev, N. Niasse, J. P. Chittenden, G. N. Hall, F. Suzuki-Vidal, G. Burdiak, A. J. Harvey-Thompson, S. N. Bland, P. De Grouchy, E. Khoory, L. Pickworth, J. Skidmore, and L. Suttle, Oblique shock structures formed during the ablation phase of aluminium wire array z-pinches, Phys. Plasmas **20**, 022705 (2013).

[23] D. H. Froula, S. H. Glenzer, N. C. J. Luhmann, and J. Sheffield, *Plasma Scattering of Electromagnetic Radiation*, 2nd ed.(Elsevier, New York, 2011).

[24] G. Espinosa, J. M. Gil, R. Rodriguez, J. G. Rubiano, M. A. Mendoza, P. Martel, E. Minguez, F. Suzuki-Vidal, S. V. Lebedev, G. F. Swadling, G. Burdiak, L. A. Pickworth, and J. Skidmore, Collisional–radiative simulations of a supersonic and radiatively cooled aluminum plasma jet, High Energy Density Phys. **17**, 74 (2015).

[25] F. Suzuki-Vidal, S. V. Lebedev, A. Ciardi, L. A. Pickworth, R. Rodriguez, J. M. Gil, G. Espinosa, P. Hartigan, G. F. Swadling, J. Skidmore, G. N. Hall, M. Bennett, S. N. Bland, G. Burdiak, P. de Grouchy, J. Music, L. Suttle, E. Hansen, and A. Frank, Bow shock fragmentation driven by a thermal instability in laboratory astrophysics experiments, Astrophys. J. **815**, 96 (2015).

[26] I. Hutchinson, *Principles of Plasma Diagnostics*, 2nd ed. (Cambridge University Press, Cambridge 2005).

[27] R. P. Drake, *High-Energy-Density Physics* (Springer-Verlag Berlin, 2006).

[28] G. Fiksel, A. F. Almagri, B. E. Chapman, V. V. Mirnov, Y. Ren, J. S. Sarff, and P. W. Terry, Mass-Dependent Ion Heating during Magnetic Reconnection in a Laboratory Plasma, Phys. Rev. Lett. **103**, 145002 (2009).

[29] Y. Ono, M. Yamada, T. Akao, T. Tajima, and R. Matsumoto, Ion Acceleration and Direct Ion Heating in Three-Component Magnetic Reconnection, Phys. Rev. Lett. **76**, 3328 (1996).

[30] M. Yamada, R. Kulsrud, and H. Ji, Magnetic reconnection, Rev. Mod. Phys. **82**, 603 (2010).

[31] S. C. Hsu, T. A. Carter, G. Fiksel, H. Ji, R. M. Kulsrud, and M. Yamada, Experimental study of ion heating and acceleration during magnetic reconnection, Phys. Plasmas **8**, 1916 (2001).

[32] D. Biskamp, *Magnetic Reconnection in Plasmas* (Cambridge University Press, Cambridge, 2000).